

Depleted Bulk Heterojunction Colloidal Quantum Dot Photovoltaics

D. Aaron R. Barkhouse, Ratan Debnath, Illan J. Kramer, David Zhitomirsky, Andras G. Pattantyus-Abraham, Larissa Levina, Lioz Etgar, Michael Grätzel, and Edward H. Sargent*

Colloidal quantum dots (CQDs) are attractive for photovoltaic (PV) and photodetector applications^[1] because they can absorb portions of the infrared (IR) spectrum that other solution-processible materials, such as conjugated polymers, generally do not. However, while CQD photovoltaic devices have already reached promising power conversion efficiencies (η) of over 5%^[2] and effectively capture almost all photons at the most strongly absorbed wavelengths, they nevertheless transmit a great deal in the IR. Both Schottky and heterojunction devices are limited by poor minority carrier diffusion lengths in CQD materials and therefore efficiently harvest photocarriers generated primarily within the depletion region.

Organic photovoltaics overcome a similar trade-off between exciton diffusion length and optical absorption length through the bulk heterojunction (BH) concept.^[3] Donor and acceptor materials are mixed on a length-scale commensurate with the exciton diffusion length in the light-absorbing phase. This has led to impressive exciton dissociation and carrier collection efficiencies that approach unity.^[4] However, the lack of a depletion region in such devices means that excitons must rely on diffusion to reach the charge-separating interface, which requires that the phase segregation occur on the 10 nm length-scale.^[4] To date, attempts at recreating the benefits of this architecture using polymer/quantum dot blends have provided only limited benefits.^[5,6] Quantum-dot-sensitized solar cells, analogous to dye-sensitized solar cells, have been explored recently as a means of overcoming this trade-off and have reached respectable conversion efficiencies,^[7–9] but those reported to date have

used quantum dots with a visible-wavelength bandgap and only a few nanometers of dots,^[10] meaning the electrodes must be made very thick in order to absorb all incident photons, thereby necessitating the use of a liquid electrolyte.^[11] As such these efforts have yet to address the limited IR sensitivity in dye-sensitized solar cells and CQD solar cells.

To maximize the efficiency of IR photon absorption and extraction in CQD devices, it would be desirable to build a nanostructured BH in which the active layer is thick enough to absorb all available photons, while ensuring that the quantum dot film remains fully depleted. We hypothesized that such a device architecture could be used to surpass the efficiency of planar depleted heterojunction (DH) CQD solar cells by allowing the device to be made thicker without sacrificing charge collection efficiency, thereby better utilizing the IR portion of the solar spectrum.

Here, we report the first solution-processed depleted bulk heterojunction (DBH) solar cells. The solar cells show an unprecedented infrared quantum efficiency in a CQD PV device. The external quantum efficiencies of the devices reach 40% at their 950 nm excitonic peak. The devices offer a record CQD PV efficiency of 5.5% under simulated AM1.5 illumination. Optimization of these large-interfacial-area devices required careful study of the charge-separating interface between the electron-accepting and donating phases. We report a study of the effects of materials processing and the resultant band offset at the heterojunction on the performance of colloidal quantum dot photovoltaics.

The DH architecture (**Figure 1**) relies on a depletion region to provide field-driven charge separation and transport. In the case of PbS CQDs ≈ 3.7 nm in diameter, the 1S electron excited state of the CQD lies about 0.3 eV above the TiO₂ conduction band edge.^[12] Thus, an additional driving force due to this favorable type-II heterojunction helps prevent the back-transfer of electrons and further assists in the collection of photoelectrons in the TiO₂. In the valence band, the highest occupied molecular orbital (HOMO) level in the PbS CQD film sees a large (>1.5 eV) discontinuity relative to the large-bandgap TiO₂, preventing hole transfer and charge recombination at the PbS/TiO₂ interface.

It was previously established that electron–hole pairs generated in the quasi-neutral CQD material beyond the depletion region are collected with a low efficiency, primarily due to the poor electron mobility in CQD films.^[13] The strategy in developing the DBH architecture is to increase the volume of the light-absorbing CQD material while ensuring that the entire CQD film is depleted, thus reducing the trade-off between

Dr. D. A. R. Barkhouse, Dr. R. Debnath, I. J. Kramer, D. Zhitomirsky,
Dr. A. G. Pattantyus-Abraham, Dr. L. Levina, Prof. E. H. Sargent
Department of Electrical and Computer Engineering
University of Toronto
10 King's College Road, Toronto, Ontario M5S 3G4, Canada
E-mail: ted.sargent@utoronto.ca

Dr. D. A. R. Barkhouse
IBM Thomas J. Watson Research Center
Kitchawan Road, Yorktown Heights, NY, 10598, USA

Dr. A. G. Pattantyus-Abraham
Quantum Solar Power Corporation
1055 W. Hastings, Ste. 300, Vancouver, BC, V6E 2E9, Canada

Dr. L. Etgar, Prof. M. Grätzel
Laboratory for Photonics and Interfaces
Institute of Chemical Sciences and Engineering
School of Basic Sciences
Swiss Federal Institute of Technology
CH-1015 Lausanne, Switzerland

DOI: 10.1002/adma.201101065

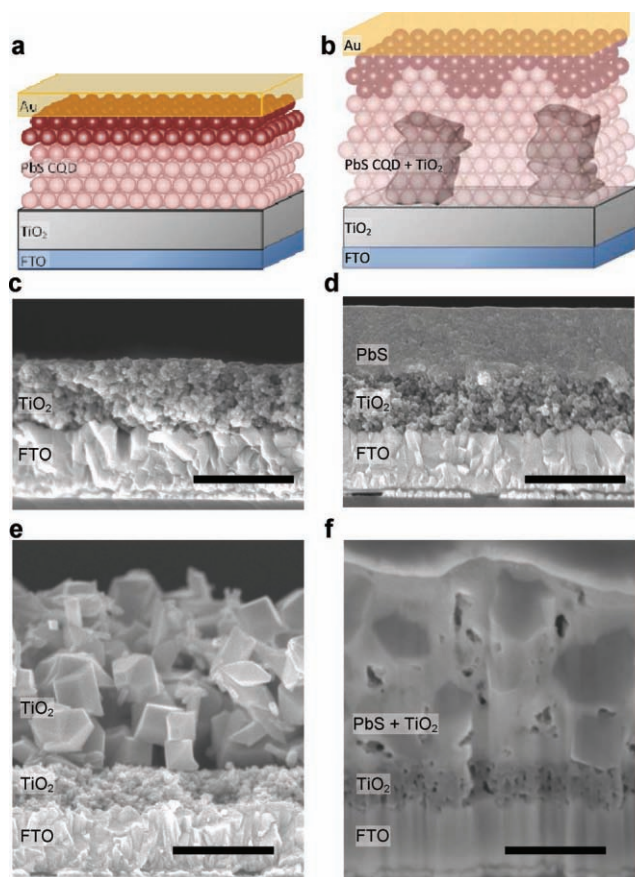


Figure 1. Schematic drawings of the cross-section of a) DH and b) DBH devices with a color gradient indicating the charge depleted portion of the device. In the DH architecture, a distinct heterointerface is formed between the light-absorbing PbS CQD and the transparent, electron-accepting TiO₂ whereas in the DBH device, a distributed heterointerface between the infiltrated CQD and TiO₂ electrode overcomes the efficiency limit of the DH device. Cross-sectional images of fluorine doped tin oxide (FTO)/TiO₂ (c,e) electrodes and FTO/TiO₂/PbS (d,f) structures for DH (c,d) and DBH (e,f) devices. In each case the scale bar is 1 μm. PbS CQDs are well infiltrated within the nanoporous TiO₂ matrix (d).

absorbance and internal quantum efficiency and leading to higher external quantum efficiency (EQE), especially in the more weakly absorbed infrared region of the solar spectrum.

DH and DBH devices were fabricated as described in detail in the Experimental Section. Electrodes were fabricated by spin-coating a paste of colloidal TiO₂ nanocrystals. In the case of DH devices, small (10–30 nm) nanocrystals were used to create a dense layer that is not easily infiltrated by PbS quantum dots in nonpolar organic solvents (Figure 1c,d). For DBH devices, a second, more porous TiO₂ layer was deposited by spin-coating a paste of large (150–250 nm) particles on top of this dense layer (Figure 1e). This serves as the template into which PbS CQDs are deposited (Figure 1f), while the denser TiO₂ underlayer prevents shunting between the PbS and fluorine-doped tin oxide (FTO).

To ensure substantially complete depletion of the CQD material, we selected the pore radius of the DBH device to be slightly smaller than the depletion width attainable in CQD/

TiO₂ planar DH devices.^[2] Capacitance–voltage measurements (Supporting Information) were used to confirm that the device was substantially depleted at zero bias. PbS CQDs were then deposited in a layer-by-layer fashion, followed by contact deposition, resulting in the final device structure shown in Figure 1d,f. The thin layer of quantum dot film between the TiO₂ and the Au electrode acts as an electron blocking layer, preventing the formation of shunts between the TiO₂ and Au.

Across the near infrared and into the short-wavelength infrared portion of the spectrum, the DBH achieved substantially higher optical absorption (Figure 2a), as intended. At the wavelength of the exciton peak, the absorption was almost two-fold higher for the DBH device compared to the DH device. By convolving with the photon flux of the AM 1.5 spectrum, we determined the expected current generation density of the respective devices (Figure 2b). The increased IR absorption of the DBH device results in a potential photocurrent enhancement of ≈30%. Disappointingly, the DBH devices built in the manner described above resulted in performance inferior to that of the planar device. Absorption increased, but the internal quantum efficiency deteriorated to an extent that more than compensated for the absorption enhancement, leading to reduced EQE (Figure 3a,b).

We sought to investigate the origins of the loss in electron collection efficiency. The short-circuit current (J_{SC}) showed a significant decrease at solar intensities compared to lower intensities (Figure 3d). This suggested that the heterointerface

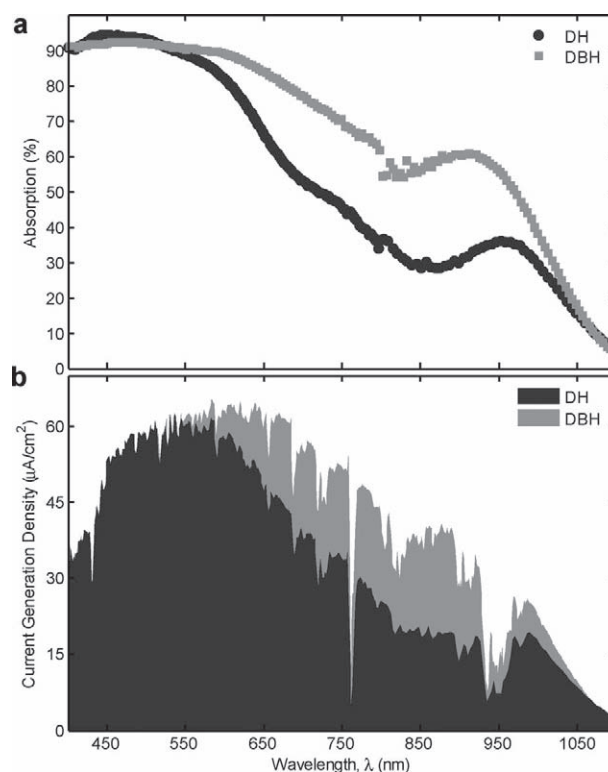


Figure 2. a) Single-pass absorption spectra of the DH and DBH devices measured in an integrating sphere. b) Expected spectral photocurrent enhancement due to enhanced absorption, yielding a 29.9% increase in the expected photocurrent.

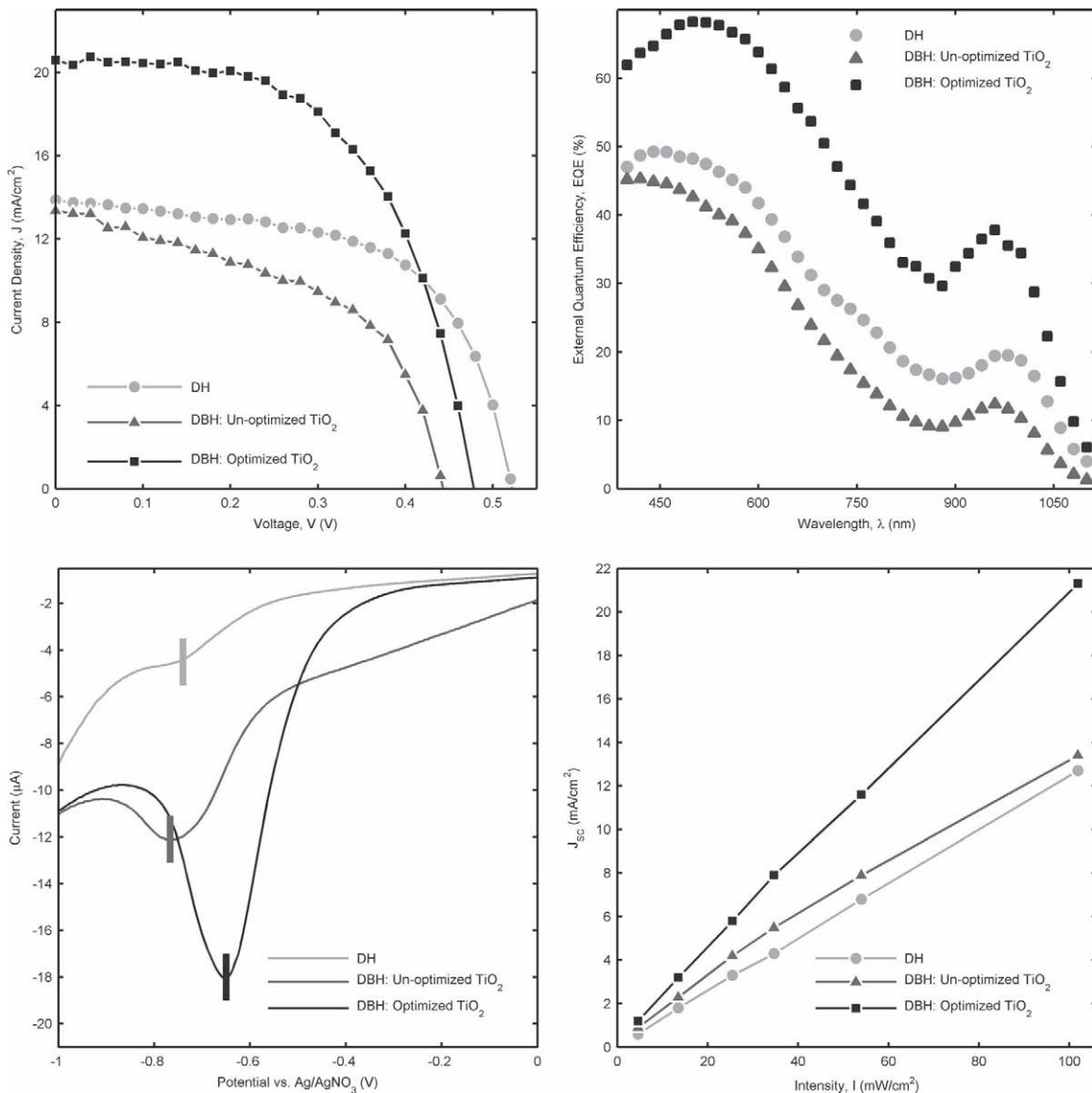


Figure 3. a) Current density vs applied bias ($J-V$) under AM 1.5 simulated solar illumination for DH, un-optimized DBH, and optimized DBH devices. b) EQE spectra for the same devices. c) CV data for various TiO₂ electrodes with vertical lines indicating the reduction potential. d) J_{sc} as a function of AM 1.5 illumination intensity indicating sub-linear behavior for the un-optimized DBH device and linear behavior for DH and optimized DBH devices.

in the DBH device had a much-reduced capacity relative to the planar device to keep charge carriers separated under high-injection conditions.

We investigated the energetic position of the conduction band edge of the DBH electrode compared to the planar electrode using cyclic voltammetry (CV) as shown in Figure 3c. These DBH electrodes had an electron affinity of -3.9 eV, almost identical to that of planar DH devices, which preserved their efficiencies up to one sun intensity (Figure 3d).

Whereas a small conduction band offset at the TiO₂-PbS QD interface can be sufficient for planar architectures where the interfacial area is relatively small, it can have a much greater impact in an architecture incorporating a high-surface-area

interface such as DBH. Figure 3d shows evidence of increased bimolecular recombination, consistent with the view that the large interfacial area produces a requirement for a larger charge-separating barrier. We therefore propose that a significant (0.3 eV or greater) conduction band offset at this interface is needed to reduce bimolecular recombination and preserve high quantum efficiency up to 1 sun.^[14]

To modify the DBH band structure to achieve the more desirable band offsets strategies were needed to reduce bimolecular recombination. We explored processes for modifying the DBH device using a range of titanium chloride (TiCl₄) treatments. We found a process that led to a short-circuit current of 20.6 mA cm⁻² for the DBH device compared to 13.9 mA cm⁻²

Table 1. Photovoltaic device performance of DH and DBH devices.

Device	V_{oc} [V]	J_{sc} [mA cm ⁻²]	FF [%]	η [%]
DH, 230 nm (control)	0.52	13.9	59	4.2
DH, 230 nm, (published) ²⁾	0.51	16.2	58	5.1
DBH, 500 nm, (unoptimized)	0.44	13.4	49	2.9
DBH, 500 nm, (optimized)	0.48	20.6	56	5.5

for its counterpart control DH planar device (16.2 mA cm⁻² for the corresponding literature DH performance^{[2])} as seen in **Table 1**. This dramatic enhancement was achieved with minor compromise to the open-circuit voltage (V_{oc} , Figure 3a) due to the deepening of the electron affinity of the optimized TiO₂ to -4.1 eV (Figure 3c). All parameters were retained up to 1 sun illumination. The resultant η of 5.5% is a record for CQD PV devices reported to date.

The EQE spectra of these devices confirm that the benefits of the DBH architecture are most striking in the infrared (Figure 3b). Here, a two- to threefold increase in EQE is achieved relative to the planar DH device. Integrating the product of the EQE and AM 1.5 spectra gives an expected J_{sc} that agrees well with the measured AM 1.5 data.

These findings suggest that a significant (a few tenths of an eV) band offset is important to the realization of efficient CQD PV devices. This is noteworthy in view of the significant driving force favoring charge separation at the heterojunction between n-type TiO₂ and p-type PbS formed through the work function difference alone, which is further augmented by a significant (0.1–0.2 eV) band offset favoring charge separation even in the unoptimized case discussed herein. The exciton binding energy in PbS CQDs is generally estimated to be ≈ 100 meV,^[15] and thus should have been overcome at low light in even the un-optimized electrode devices. Taken together, these findings indicate that the most effective heterojunction materials pairings for quantum dots need to offer ≈ 0.2 eV worth of excess charge-separating energy over and above the exciton binding energy. Unfortunately, this requirement imposes a further limitation on a V_{oc} that is already significantly lower than one might hope for in an ≈ 1.3 eV bandgap active material solar cell. This excessive offset may be required due to ensure that electrons can be injected into the TiO₂ from the lowest-lying state in the inhomogeneous quantum dot ensemble, as electrons should naturally percolate to the largest dots (those with the smallest bandgap). By narrowing the size distribution in the dots, and bringing the smallest bandgap dots closer to the nominal bandgap of the quantum dot layer, it may be possible to reduce the size of the conduction band offset while maintaining efficient charge injection.

We conclude with a discussion of the conditions necessary to reach higher power conversion efficiencies from CQD PV devices. The devices reported herein, employing a 1.3 eV bandgap, achieve 20 mA cm⁻² short-circuit current density, whereas the ideal single-junction device with the same bandgap can in principle reach up to 37 mA cm⁻². To more closely approach this ideal will demand complete absorption and efficient extraction across the full range of wavelengths from 400 to 950 nm. This will require an ≈ 2 μ m thick nanoporous

TiO₂ electrode if half of the volume of the porous electrode is filled with CQDs. For a minority carrier life time of 1 μ s, efficient extraction of this distance, which is necessary both to J_{sc} and the fill factor (FF), will require an electron mobility in the TiO₂ and a hole mobility in the CQD phase, each exceeding 1 cm² V⁻¹ s⁻¹.

There exists considerable room for improvement in V_{oc} to increase from its present ≈ 0.5 V to approach the ideal ≈ 1 V possible in principle in an ≈ 1.3 eV solar cell. Reducing the excess band offset at the interface may provide up to a 0.3 V gain in V_{oc} . The remaining improvement will come from removal of the shunts and recombination current that together account for the undesirably high reverse-saturation current density in these devices.

In summary, the DBH device enables enhanced absorption without compromising extraction leading to an actual J_{sc} enhancement approaching 30% relative to a planar device. This improvement is in good agreement with the gain expected from current generation calculations. This architecture is also susceptible to bimolecular recombination due to the high surface area of the heterojunction. In order to reduce this performance limiting process we employed surface modifications that led to a record power conversion efficiency of 5.5%.

Experimental Section

Chemicals and Materials: Lead oxide (PbO) (99.9%), bis(trimethylsilyl) sulphide (TMS, synthesis grade), oleic acid (90%), 1-octadecene (ODE, 90%), 3-mercaptopropionic acid (MPA, 99%), ethanol, titanium (IV) chloride, Triton X-100, tetrabutylammonium hexafluorophosphate, ferrocene, and all solvents (anhydrous grade) were purchased from Sigma-Aldrich.

Fluorine-doped tin oxide (FTO) coated glass substrates (2.5 \times 2.5 cm², Pilkington TEC 15) were obtained from Hartford Glass. TiO₂ nanoparticles (DS-90) were obtained from Dyesol, Inc. Au (99.99%) and Ag (99.99%) pallets were obtained from Kurt J. Lesker, Inc.

PbS Qd Synthesis and Purification: All chemicals were used as-received unless stated otherwise. TMS (0.18 g, 1 mol) was added to ODE (10 mL), which had been dried and degassed by heating to 80 °C under vacuum for 24 h. A mixture of oleic acid (1.34 g, 4.8 mmol), PbO (0.45 g, 2.0 mmol), and ODE (14.2 g, 56.2 mmol) was heated to 95 °C under vacuum for 16 h then placed under Ar. The flask temperature was increased to 125 °C and the TMS/ODE mixture was injected. After injection, the temperature lowered to ≈ 95 °C and the flask was allowed to cool gradually to 36 °C.

The nanocrystals were precipitated with distilled acetone (50 mL) and centrifuged. After discarding the supernatant, the precipitate was redispersed in toluene. The nanocrystals were precipitated again with acetone (20 mL), centrifuged (5 min), dried, and finally dispersed in toluene (≈ 350 mg mL⁻¹).

PbS nanocrystals were then precipitated with methanol and dried under vacuum once the supernatant was removed. They were then redispersed in toluene (100 mg mL⁻¹). This process was repeated twice more, with the final redispersion in octane (50 mg mL⁻¹).

Electrode Preparation: TiO₂ nanoparticle paste (DSL90-T, Dyesol) was diluted in ethanol and spin-coated onto FTO substrates. For DH devices, the nanoparticles were diluted with ethanol (1:3 by weight), spun at 1500 rpm, and placed on a hotplate preheated to 120 °C. For DBH devices, they were diluted in ethanol (1:5 by weight), spun at 2000 rpm, and placed on hotplate at room temperature. All substrates were then heated at 200 °C for 15 min and 400 °C for 60 min only for DH devices. For DBH devices, a paste of large (150–250 nm diameter) TiO₂ nanoparticles (WER2-0, Dyesol) was diluted in ethanol and spin-coated with the dilution and spin

speed chosen to give the desired layer thickness. The electrodes were then heated to 200 °C for 15 min and 400 °C for 60 min.

All substrates underwent TiCl_4 treatment (60 mm for DH and un-optimized DBH, 240 mm for optimized DBH) solution in deionized (DI) water at 70 °C for 30 min. Substrates were removed, rinsed with DI water, and fired at 520 °C for 60 min. Aside from contact evaporation, all other fabrication was carried out in a fume hood in air ambient.

Device Fabrication and Characterization: PbS CQDs in octane (50 mg mL^{-1}) were applied to the substrates in a layer-by-layer fashion. Two drops of CQDs were dispensed onto the substrate through a $0.2 \mu\text{m}$ filter, and after 3 s the substrate was spun at 2500 rpm for 15 s. Five drops of MPA:methanol solution (10% by volume) solution were applied, and the substrate was spun again after a 3 s wait. Two rinse steps with methanol were applied, and the process was repeated until the desired film thickness had been reached.

Top contacts were applied by thermal evaporation in Angstrom Engineering Åmod deposition system in an Innovative Technology glovebox, at a base pressure of 1×10^{-7} mbar, and consisted of gold (30 nm) followed by silver (270 nm) deposited through a shadow mask with 2.78 mm circular openings, giving 0.06 cm^2 contacts.

AM 1.5 performance characterization was performed with a class A solar simulator (Science Tech). Devices were illuminated through a 2.5 mm diameter aperture to avoid overestimation of photocurrent. Bias sweeps were performed with a Keithley 2400 digital multimeter, and testing was performed in a sealed, nitrogen-purged test box. Neutral density metal mesh filters were used for intensity dependence measurements.

Absorption spectroscopy was carried out in a Cary 500 UV-Vis-IR Scan spectrophotometer using an integrating sphere. Scanning electron microscopy was performed on cross-sectional samples prepared by mechanical fracture of electrodes/devices.

EQE measurements used a xenon arc lamp coupled to a Jobin Yvon Triax 320 monochromator to provide monochromatic illumination with a 40 nm bandwidth.

Electrochemical analysis of the TiO_2 was performed using a standard three-electrode cell in combination with PamSens EmStat potentiostat. Silver/silver nitrate (Ag/AgNO_3 0.1 M in acetonitrile) was used as a reference electrode and tetrabutylammonium hexafluorophosphate was used as the electrolyte. The Ag/AgNO_3 electrode was calibrated by measuring CV data for ferrocene.

Supporting Information

Supporting Information is available from the Wiley Online Library or from the author.

Acknowledgements

D.A.R.B and R.D. contributed equally to this work. This publication is based on work supported in part by Award No. KUS-I1-009-21, made by King Abdullah University of Science and Technology (KAUST). The authors thank Angstrom Engineering and Innovative Technologies for useful discussions regarding material deposition methods and control

of the glovebox environment, respectively. D.A.R.B. would like to thank the Ontario Postdoctoral Fellowship program and the Natural Sciences and Engineering Research Council for financial support. R.D. and I.J.K. acknowledge the financial support through e8/MITACS Elevate Strategic fellowship and the Queen Elizabeth II/Ricoh Canada Graduate Scholarship in Science and Technology, respectively. L.E. acknowledges the Marie Curie Actions—Intra-European Fellowships (FP7-PEOPLE-2009-IEF) under grant agreement n° 252228. The authors would also like to acknowledge the technical assistance and scientific guidance of L. Brzozowski, E. Palmiano, R. Wolowicz, and D. Kopilovic.

Received: March 23, 2011

Revised: April 25, 2011

Published online:

- [1] G. Konstantatos, E. H. Sargent, *Nat. Nanotechnol.* **2010**, *5*, 391.
- [2] A. G. Pattantyus-Abraham, I. J. Kramer, A. R. Barkhouse, X. Wang, G. Konstantatos, R. Debnath, L. Levina, I. Raabe, M. K. Nazeeruddin, M. Grätzel, E. H. Sargent, *ACS Nano* **2010**, *4*, 3374.
- [3] A. Pivrikas, N. S. Saricifci, G. Juška, R. Österbacka, *Prog. Photo-voltaics* **2007**, *15*, 677.
- [4] S. H. Park, A. Roy, S. Beaupre, S. Cho, N. Coates, J. S. Moon, D. Moses, M. Leclerc, K. Lee, A. J. Heeger, *Nat. Photonics* **2009**, *3*, 297.
- [5] N. C. Greenham, X. Peng, A. P. Alivisatos, *Phys. Rev. B* **1996**, *54*, 17628.
- [6] S. A. McDonald, G. Konstantatos, S. Zhang, P. W. Cyr, E. J. D. Klem, L. Levina, E. H. Sargent, *Nat. Mater.* **2005**, *4*, 138.
- [7] E. M. Barea, M. Shalom, S. Giménez, I. Hod, I. n. Mora-Seró, A. Zaban, J. Bisquert, *J. Am. Chem. Soc.* **2010**, *132*, 6834.
- [8] H. Lee, M. Wang, P. Chen, D. R. Gamelin, S. M. Zakeeruddin, M. Grätzel, M. K. Nazeeruddin, *Nano Lett.* **2009**, *9*, 4221.
- [9] Y.-L. Lee, Y.-S. Lo, *Adv. Funct. Mater.* **2009**, *19*, 604.
- [10] H. Lee, H. C. Leventis, S.-J. Moon, P. Chen, S. Ito, S. A. Haque, T. Torres, F. Nüesch, T. Geiger, S. M. Zakeeruddin, M. Grätzel, M. K. Nazeeruddin, *Adv. Funct. Mater.* **2009**, *19*, 2735.
- [11] B. O'Regan, M. Grätzel, *Nature* **1991**, *353*, 737.
- [12] B.-R. Hyun, Y.-W. Zhong, A. C. Bartnik, L. Sun, H. D. Abruna, F. W. Wise, J. D. Goodreau, J. R. Matthews, T. M. Leslie, N. F. Borrelli, *ACS Nano* **2008**, *2*, 2206.
- [13] K. W. Johnston, A. G. Pattantyus-Abraham, J. P. Clifford, S. H. Myrskog, S. Hoogland, H. Shukla, E. J. D. Klem, L. Levina, E. H. Sargent, *Appl. Phys. Lett.* **2008**, *92*, 122111.
- [14] B. C. O'Regan, J. R. Durrant, P. M. Sommeling, N. J. Bakker, *J. Phys. Chem. C* **2007**, *111*, 14001.
- [15] J. J. Choi, J. Luria, B.-R. Hyun, A. C. Bartnik, L. Sun, Y.-F. Lim, J. A. Marohn, F. W. Wise, T. Hanrath, *Nano Lett.* **2010**, *10*, 1805.